Neutron Radiative Capture in Na, Al, Fe, and Ni from 1 to 200 keV*

R. W. HOCKENBURY, Z. M. BARTOLOME, J. R. TATARCZUK, W. R. MOYER, AND R. C. BLOCK†
Nuclear Engineering and Science Division, Rensselaer Polytechnic Institute, Troy, New York 12181

(Received 10 May 1968)

Neutron radiative capture in Na, Al, Fe, and Ni has been measured from 100 eV to 200 keV with a 1.25-m-diam liquid scintillator detector at the Rensselaer LINAC Laboratory. Radiation widths were determined for those resonances whose neutron widths are well known, while the resonance capture areas ($\sigma_0\Gamma_\gamma$) were determined for most of the other resonances. Considerably more resonances were observed in the capture measurements upon Fe and Ni than had been observed in total cross-section measurements. It is reasonable to assign most if not all of these previously undetected resonances to p-wave neutrons, and from these data p-wave strength functions of $(0.10\pm0.04)\times10^{-4}$ and $(0.04\pm0.03)\times10^{-4}$ were determined, respectively, for ^{56}Fe and ^{58}Ni. These strength functions are probably just upper limits to the true p-wave strength functions and are an order of magnitude smaller than optical-model predictions.

I. INTRODUCTION

THE study of neutron radiative-capture cross sections provides information pertaining to the fields of nuclear structure, nucleogenesis, and reactor technology. Capture measurements can be combined with total cross-section measurements to determine detailed information on nuclear resonance structure, in particular, the resonance energies, spins, and widths. From these resonance parameters, information on strength functions, distributions of widths and spacings, etc., can be extracted.

The validity of the s process in nucleogenesis[1] can be studied by knowing the capture cross section. Since stellar temperatures correspond to neutron energies of tens of keV, capture cross sections in this energy range are needed for many stable nuclei of mass $A \gtrsim 50$.

Accurate radiative-capture cross sections are also needed for the design of fast reactors. These data enter into the calculation of breeding ratios, shielding, critical masses, temperature coefficients of reactivity, and neutron energy spectra. Since reactor structures are "thick" samples, capture in the strong s-wave resonances saturates and thus the weaker p-wave resonances will contribute to the total capture rate. Sodium and aluminum, iron and nickel are used as a coolant and as structural materials, respectively, in fast reactors. For these nuclei in the keV region, neutron scattering is by far the dominant process for s-wave resonances. Good energy resolution is required to resolve the weaker p-wave resonances.

Capture cross sections have been measured before by the following techniques (see Ref. 2 for an excellent review of this subject): (1) activation; (2) shell-transmission method; (3) in-pile techniques; (4) mass spectrometry; and (5) prompt γ-ray detection. However, only the method of prompt γ-ray detection is suitable for high-resolution capture measurements in the keV range. For this method, scintillation detectors are frequently used to detect the prompt γ rays emitted from the nucleus after neutron capture. Present methods attempt to achieve detector efficiencies which are independent of the γ-cascade scheme. In one such detector, called the Moxon-Rae detector,[3] the capture γ rays are incident on a graphite converter plate. The detection efficiency is proportional to γ-ray energy and thus is independent of the decay scheme. Modifications[4] have been made to improve the linearity and increase the absolute efficiency, which is about 3.5% with a graphite converter.

Another class of prompt γ detectors are the large liquid scintillators. The efficiency of this type of detector is relatively independent of cascade scheme since even the most energetic ($\sim$9 MeV) γ rays have a high probability of interacting in the detector. With a suitable scintillator mixture and good neutron shielding, this detector is essentially insensitive to scattered neutrons. These detectors typically have a very fast time response, 4–20 nsec, depending on the electronics system used with them.

The purpose of this work was to measure neutron capture in samples of Na, Al, Fe, and Ni over an energy range from approximately 100 eV to 200 keV. In those resonances where the neutron width is known from total cross-section measurements and $\Gamma_n \gg \Gamma_\gamma$, where Γ_n and Γ_γ are, respectively, the resonance partial widths for neutron emission and neutron capture, the radiation width is determined from the capture data. In the other general class of resonances, many of which have been seen for the first time in this experiment, $\Gamma_n \lesssim \Gamma_\gamma$. If $\Gamma_n \ll \Gamma_\gamma$, a value of $g\Gamma_n$ is obtained from the area under the capture resonance, where g is the statistical weight factor; for the remaining resonances, $g\Gamma_n\Gamma_\gamma/\Gamma$ is determined from the resonance capture

* Taken in part from the thesis submitted to Rensselaer Polytechnic Institute by R. W. Hockenbury in August, 1967, in partial fulfillment of the requirements for the Ph.D. degree. Supported by Contract No. AT(30-3-328) with the U.S. Atomic Energy Commission.

† This author carried out the initial part of this research while he was a member of the Physics Division of the Oak Ridge National Laboratory.

[1] G. I. Bell, Rev. Mod. Phys. **39**, 59 (1967).

[2] J. B. Marion and J. L. Fowler, *Fast Neutron Physics* (Interscience Publishers, Inc., New York, 1963), Part II.

[3] M. C. Moxon and E. R. Rae, in *Proceedings of the Symposium on Neutron Time-of-Flight Methods, Saclay, France, 1961*, edited by J. Spaepen (EURATOM, Brussels, 1961) p. 439.

[4] H. Weigmann, G. Carraro, and K. H. Bockhoff, Nucl. Instr. Methods **50**, 267 (1967).

area. From these data a value of the p-wave strength function is obtained for ^{56}Fe and ^{58}Ni which is an order of magnitude lower than predicted by the optical model.[5]

For these measurements, the Rensselaer electron linear accelerator was used for the neutron source and the Oak Ridge National Laboratory (ORNL) 1.25-m-diam liquid scintillation detector[6] was used to detect capture. The capture detector to be described is extremely insensitive to scattered neutrons. Comparisons of the present capture data and transmission data[7] show that this capture detector has a sensitivity for detecting weak resonances about 50 times greater than the neutron detectors used in transmission experiments. These two features of the present capture detector, insensitivity to scattered neutrons and high efficiency for detection of weak resonances together with improvements in the (1) neutron-production target and moderator geometry, (2) neutron collimation, and (3) detector electronics, made it possible to measure neutron capture to 200 keV.

II. EXPERIMENT

A. Neutron Source

Electrons from the Rensselaer linear accelerator strike a water-cooled aluminum-jacketed tantalum target (Fig. 1), producing an intense burst of bremsstrahlung which in turn yields an evaporation-type photoneutron spectrum. For these experiments, the electron pulse width was varied from 10 to 100 nsec. Peak electron currents varied between 1.2 and 2.0 A and electron energies varied from 45 to 60 MeV.

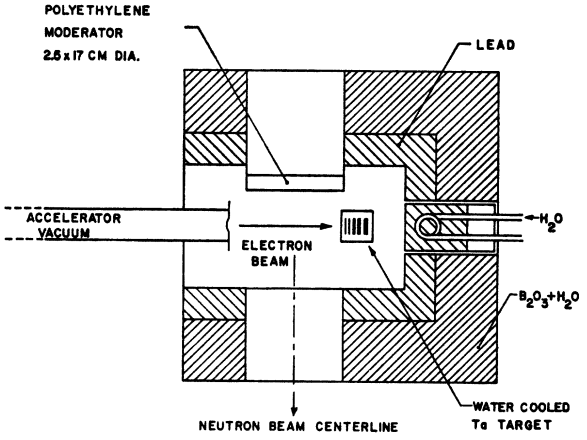

FIG. 1. Target—Moderator geometry.

[5] C. Slavik (private communication).

[6] R. C. Block, G. G. Slaughter, L. W. Weston, and F. C. Vonderlage, in *Proceedings of the Symposium on Neutron Time-of-Flight Methods, Saclay, France, 1961*, edited by J. Spaepen (EURATOM Brussels, 1961) p. 203.

[7] Neutron Cross Sections, compiled by M. D. Goldberg, F. Mughabghab, B. A. Magurno, and V. M. May, Brookhaven National Laboratory Report No. BNL-325, 2nd ed., Suppl. No. 2, Vol. III A (unpublished).

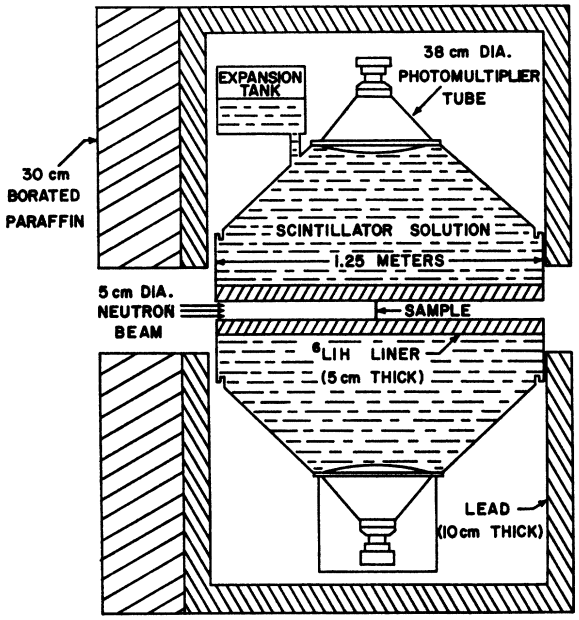

FIG. 2. Neutron capture detector.

The arrangement of electron beam, electron target, and polyethylene moderator is shown in Fig. 1. A 2.5-cm×17-cm-diam polyethylene disk, placed at ~135° relative to the target, is used to moderate the high-energy photoneutrons into the resonance energy region. This target-moderator geometry resulted from a series of experiments designed to optimize the electronic recovery from the intense beam flash with little sacrifice in neutron intensity. With this geometry, only the low-intensity bremsstrahlung emitted at ~135° strikes the moderator, and these photons in turn must Compton scatter by ~135° in the moderator to be detected as beam flash in the scintillation detector. A 0.32-cm-thick lead filter is placed in the neutron flight tube ~12 m away to absorb these low-energy Compton-scattered photons.

B. Capture Detector

Figure 2 shows the capture detector used in these experiments. This detector was located 25.44 m from the polyethylene moderator target, and the neutron beam was collimated to 5-cm diam at the center of the detector. Details of the collimation may be found in the thesis by Hockenbury.[8] The detector[6] was constructed at the Oak Ridge National Laboratory and consists of sheet steel in the form of two truncated cones and a cylinder welded together to approximate a spherical shape 1.25 m in diameter. A neutron beam hole 17.7 cm in diameter passes through the center of the detector. The interior of the detector is coated with reflecting Al_2O_3 (Linde α-alumina) bonded with sodium silicate

[8] R. W. Hockenbury, thesis, Rensselaer Polytechnic Institute, 1967 (unpublished).

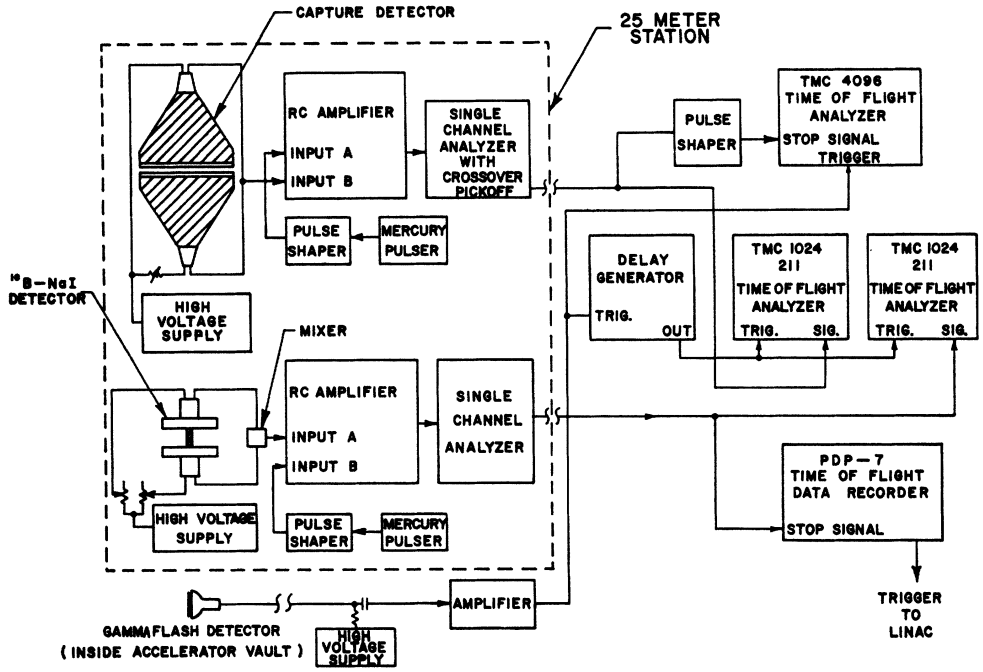

FIG. 3. Block diagram of electronics system.

to improve the light-collection efficiency. The detector is surrounded by a 10-cm-thick Pb shield which reduces the cosmic-ray background counting rate by about a factor of 3. The side facing the beam also is shielded by 30 cm of borated paraffin to absorb neutrons which may be scattered out of the direct beam by the collimator system. A ^{6}LiH liner, 5 cm thick, is placed inside the detector to absorb neutrons scattered by the sample.

The scintillating solution is composed of 1100 liters of triple-distilled xylene, 4 g/liter of *p*-terphenyl, and 0.05 g/liter of α-NPO. Neutrons which do enter the scintillant may be captured by the hydrogen-producing troublesome 2.2-MeV γ rays. This is suppressed by adding boron in the form of methyl borate to the solution. A loading of 0.0056 boron atom per hydrogen atom reduces the probability of hydrogen capture by a factor of about 14. Capture in the boron results in the emission of a 480-keV γ ray ($\sim$92% of the time) which is well below the normal operating bias of the detector.

Two K1328 Dumont 38-cm-diam photomultiplier tubes are mounted on the detector in direct contact with the scintillator. Viton *A* O-rings are used to obtain a tight seal, since Viton is not attacked by xylene. Pulses from two photomultiplier tubes are summed, amplified, and fed to a wide-window discriminator whose limits correspond to photon energies between 3 and 15 MeV. A cosmic-ray background of $\sim$100 counts per second is observed at this bias. Discriminator pulses are then sent to TMC 4096 and 1024-channel time-of-flight analyzers via 100 m of RG-62 doubly shielded coaxial cable. The photon energy calibration of the discriminator is determined by placing a ^{60}Co source inside the detector and observing the position of the 2.5-MeV sum peak. A block diagram of the detector electronics is shown in Fig. 3. The timing of the discriminator output pulse was derived from the zero crossover point of the amplifier pulses, thus making the timing relatively insensitive to pulse amplitude. A stilbene crystal mounted on a photomultiplier inside the accelerator hall provided a fast ($\sim$5-nsec risetime) γ flash signal to start the time analyzers. The over-all jitter of the capture detector plus auxiliary electronics was experimentally determined to be $\sim$30 nsec, resulting in a best resolution of $\sim$1.3 nsec/m. The dead times of the discriminator and the time-of-flight analyzer were 0.8 and 1.28 μsec, respectively. Since a pulse was recorded almost every Linac cycle from the beam flash, a dead space could occur in the data corresponding to high-neutron energies. This situation was alleviated by artificially pulsing the discriminator through the amplifier at times just preceding the electron pulse. Thus the electronics recovered shortly after the electron pulse and enabled data to be obtained at higher neutron energies.

C. Neutron-Flux Detector

The relative neutron flux as a function of energy was determined by using a $^{10}B_4C$-NaI neutron detector. Neutrons captured in ^{10}B produce 480-keV γ rays via the $^{10}B(n, \alpha\gamma)^{7}Li$ reaction ($\sim$92% of the time). These γ rays are detected by an assembly of two 5-cm-thick by 20-cm-diam NaI crystals each mounted upon a

58AVP photomultiplier tube. This detector was located inside a 10-cm-thick lead shield at a 28-m flight path just behind the neutron capture detector. The neutron detector electronics system is shown in Fig. 3.

D. Samples

The metallic sodium samples, prepared at the Oak Ridge National Laboratory, were pressed and cut into disks which were then sealed in Al containers consisting of a flat ring and two thin windows. The diameter of the sodium itself was 7.6 cm. The Al, Fe, and Ni samples were either machined or cut from pure metal sheets. The diameter of all these samples was 7.93 cm. One Ni sample was pressed from powder and sealed in an Al container similar to the ones used for sodium. The thicknesses of the samples are listed in Table I. The weights and enrichments of the separated isotopically enriched samples of Fe and Ni are listed in Table II. With the exception of the metallic isotopes of ^{56}Fe and ^{57}Fe, all the isotopes were used as powdered oxides resting in their glass containers.

TABLE I. Capture samples.

Element	Thickness (10^{-2} atom/b)
Sodium	0.2031
	0.2855
	0.6432
	1.1165
	2.1976
	4.1793
Aluminum	3.7223
	11.7730
Iron (Armco)	0.6799
	1.3642
	5.3876
	10.7644
Nickel	0.4967
	2.8898
	4.8109

E. General Experimental Method

A typical capture measurement consisted of a 3-h run with a thin gold monitor foil on the front face of the capture sample. The time-of-flight analyzers were read out at 3-h intervals for the longer runs. Neutron-flux measurements were made at frequent intervals interspersed with the capture runs. One iron sample (4.994-gm/cm^2 thick) was run at intervals throughout the experiment to provide an additional check on reproducibility of results. Time-independent background measurements of both detectors were made with the beam injector turned off. This provided a constant check of detector biases.

TABLE II. Separated isotopes.

Isotope	Atom percent 54	56	57	58	Weight (g)
^{56}Fe	0.118	99.70	0.147	0.036	72.6
^{57}Fe	0.14	8.53	91.19	0.14	4.587
^{58}Fe	0.45	15.83	1.6	82.12	7.149

Isotope	Atom percent 58	60	61	62	64	Weight (g)
^{58}Ni	99.89	0.11	0.02	0.02	0.02	33.119
^{60}Ni	0.21	99.79	0.05	0.05	0.05	100.0
^{61}Ni	1.62	5.18	92.11	1.08	0.05	16.0
^{64}Ni	0.85	0.56	0.05	0.39	98.15	15.240

The true "time zero" of the analyzers was found by placing 10 cm of lead in the neutron beam and reducing the electron intensity. Under these conditions a time-zero peak corresponding to the γ flash is recorded in the analyzers with no dead-time distortion. The 83-nsec flight time of the photons is not negligible and was included in the calculation of neutron energies.

III. ANALYSIS

A. Capture Yield

The basic quantity obtained from this partial cross-section experiment is called the capture "yield" and

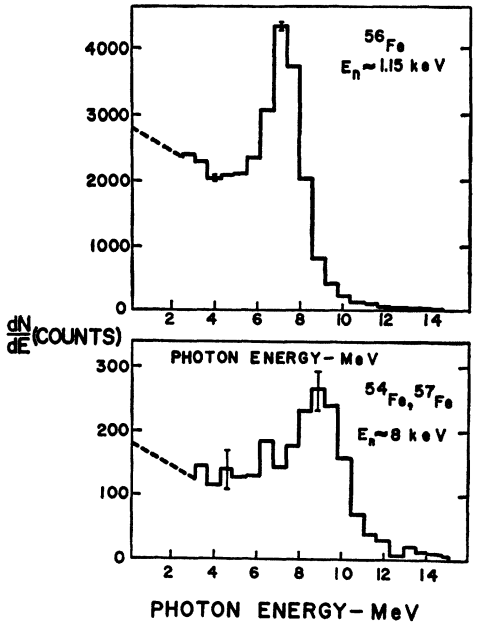

FIG. 4. Capture-γ pulse-height spectra of ^{54}Fe, ^{56}Fe, and ^{57}Fe.

TABLE III. Capture detector efficiency.

Isotope	Binding energy[a] (MeV)	Spectrum fraction	Cascade efficiency	Total efficiency
^{23}Na	6.958	0.62±0.02	0.98±0.02	0.601±0.030
^{27}Al	7.723	0.68±0.03	0.90±0.01	0.61±0.032
^{54}Fe	9.297	0.76±0.03	0.80±0.02	0.61±0.035
^{56}Fe	7.638	0.69±0.03	0.87±0.02	0.60±0.035
^{57}Fe	10.03	0.76±0.03	0.80±0.02	0.61±0.035
^{58}Fe	6.6	...	...	0.60[b]
^{58}Ni	8.998	0.75±0.03	0.83±0.02	0.63±0.035
^{60}Ni	7.8	0.71±0.03	0.85±0.02	0.60±0.035
^{61}Ni	10.626	0.75±0.03	...	0.63±0.03[b]
^{62}Ni	6.825	...	...	0.60[b]
^{64}Ni	6.13	...	...	0.605[b]
^{107}Ag	7.27	0.73±0.01	0.98±0.01	0.72±0.015
^{109}Ag	6.6			

[a] Reference 12. [b] Assumed from binding energy.

is defined as

$$Y_{xi}(E)=\frac{\text{(number of neutron captures)}}{\text{(number of incident neutrons)}}, \quad (1)$$

where $Y_{xi}(E)$ is the capture yield of sample x in time-of-flight channel i corresponding to incident neutron energy E. This yield can be written in terms of the detector counting data and detector efficiencies:

$$Y_{xi}(E)=(C-C_B)_i/\eta_{xi}KA_{\mathrm{Au}}\phi_{\mathrm{Ri}}, \quad (2)$$

where $(C-C_B)_i$= net capture detector counts recorded in channel i (corrected for background and dead-time effects), η_{xi}=capture detector efficiency for sample x in channel i (corresponding to capture of neutrons of incident energy E), ϕ_{Ri}=relative number of incident neutrons in channel i, A_{Au}=capture detector counts integrated over the 60.2-eV Au resonance, and K=a normalization constant relating the absolute number of incident neutrons at 5.19 eV to the integrated capture counts of the 60.2-eV Au resonance.

The absolute number of neutrons per time channel, $KA_{\mathrm{Au}}\phi_{\mathrm{Ri}}$, is obtained in the following manner:

1. The relative number of neutrons per channel is determined with a $^{10}B_4C$-NaI detector whose relative efficiency is calculated from the ^{10}B cross section as a function of neutron energy.[9]

2. The absolute number of neutrons is determined at one energy by the saturated resonance method,[10] using the 5.19-eV Ag resonance.

3. A thin Au monitor foil was always left inside the capture detector and the integrated resonance capture from the 60.2-eV Au resonance was used as a flux monitor. An auxiliary experiment was performed to calibrate the Au monitor resonance capture with the saturated resonance capture near 5.19 eV from a thick Ag sample.

$(C-C_B)_i$—*Capture Detector Data*

The number of capture counts versus time of flight was recorded for various sample thicknesses and running conditions. Dead-time corrections were made, assuming nonextended dead-time losses. Background runs were interspersed between capture runs. The time-independent portion of the background was measured at frequent intervals with the accelerator turned off. The time-dependent background is attributed to:

(1) high-energy (MeV) neutrons scattered by the sample into the detector at times immediately after the electron pulse,

(2) neutron scattering and leakage in the collimation and shielding, and

(3) neutron-energy degradation in the collimation system.

The time-dependent part of the background was determined for each sample by placing in the beam samples of Co, Mn, Na, and Al which have "black" resonances at 0.132, 0.337, 2.37, 2.85, 35, and 88 keV.

η_{xi}—*Capture Detector Efficiency*

Neutron capture-γ pulse-height distributions were measured for several resonances in each sample by using the analyzer in the time-of-flight versus pulse-height mode. The fraction of scintillator events passed

[9] R. W. Hockenbury, Z. M. Bartolome, W. R. Moyer, and R. C. Block, Linear Accelerator Progress Report, 1966, Rensselaer Polytechnic Institute (unpublished).

[10] E. R. Rae and E. M. Bowey, J. Nucl. Energy 4, 179 (1957).

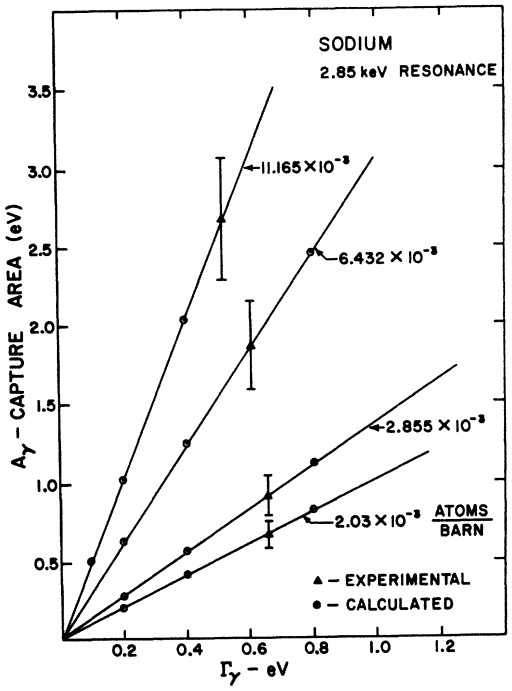

FIG. 5. Integrated capture yield A_γ versus Γ_γ for the 2.85-keV Na resonance.

by the discriminator, or "spectrum fraction,"[11] was determined from these pulse-height data.

A cascade correction is also made for those photons which pass through the detector without interacting, assuming that the capture-γ de-excitation scheme is the same for resonance capture as for thermal-neutron capture.[12] Since the detector pulse-height resolution is observed to be $\sim$40% (for 1.6-MeV photons) and since the cascade scheme comes in as a small correction, this is a reasonable assumption.[13] The total efficiency is then the product of the spectrum fraction and the cascade correction.

For the thicker samples, there is the possibility that the capture γ rays may interact before leaving the sample. Using the photon cross sections of Siegbahn[14] for iron, calculations were made of the probability of self-absorption of the capture γ rays by the samples. Since there is very little absorption of photons for typical energies encountered, those few photons that interact in the sample are primarily scattered, thus losing some energy. This only shifts them to a lower energy in the pulse-height spectrum; thus they are included in the spectrum fraction since the spectrum fraction was measured for the samples actually used.

Typical pulse-height spectra are shown in Fig. 4 for capture in the 1.15-keV ^{56}Fe resonance and the 8-keV region for ^{54}Fe and ^{57}Fe resonances. These spectra are characterized by a prominent peak near the neutron binding energy due to the large number of high-energy photons emitted following neutron capture. Appendix I contains a discussion of spectrum fractions for three principal types of de-excitation schemes and for various binding energies. Table III gives the measured spectrum fraction, computed cascade efficiency, and the total efficiency for the samples investigated.

Relative Neutron Flux

The neutron-detector data were corrected for dead-time losses, and the time-independent and time-dependent background were determined in a manner similar to that used for the capture detector.

The relative efficiency of the neutron detector is defined as the number of 480-keV photons emitted from the 1.2-cm-thick $^{10}B_4C$ slab per incident neutron. Since the $^{10}B_4C$ slab is not "black" at all energies, a multiple scattering correction[9] is necessary. This correction also allows for those photons which undergo scattering and subsequent energy degradation in the $^{10}B_4C$ slab. These calculations were performed using the recent absorption and scattering cross sections of ^{10}B as given in Ref. 15.

The multiple scattering correction was checked experimentally in a separate measurement using a "thin" ^{10}B sample for which the scattering correction was very small. Both the 1.2-cm-thick $^{10}B_4C$ slab and thin ^{10}B slab data yielded the same value of neutron flux to within the experimental accuracy of $\pm$3%.

Flight-Path Correction

The neutron flux was measured at a flight path of 28.05 m while the capture samples were located at

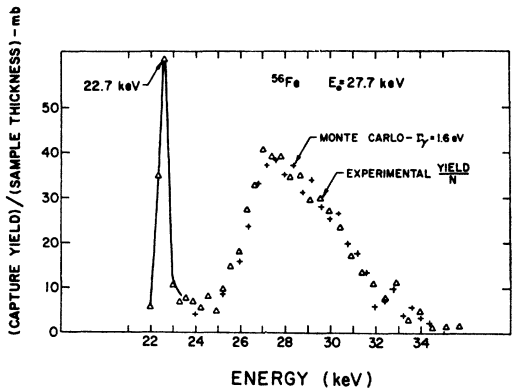

FIG. 6. (Capture yield)/(sample thickness) for the 27.7-keV resonance in ^{56}Fe.

[11] J. H. Gibbons, R. L. Macklin, P. D. Miller, and J. H. Neiler, Phys. Rev. **122**, 182 (1961).

[12] L. V. Groshev, V. N. Lutsenko, A. M. Demidov, and V. I. Pelekhov, *Atlas of γ-Ray Spectra From Radiative Capture of Thermal Neutrons* (Pergamon Press, Inc., New York, 1959).

[13] Actually, the resonance-capture pulse-height spectra were similar to the thermal spectra, indicating that both are characterized by the same "hardness" of photons, and hence the same correction for photon leakage.

[14] K. Siegbahn, *Beta and Gamma Ray Spectroscopy* (Interscience Publishers, Inc., New York, 1955).

[15] K. M. Diment, Atomic Energy Research Establishment (England) Report No. AERE-R5224, 1967 (unpublished).

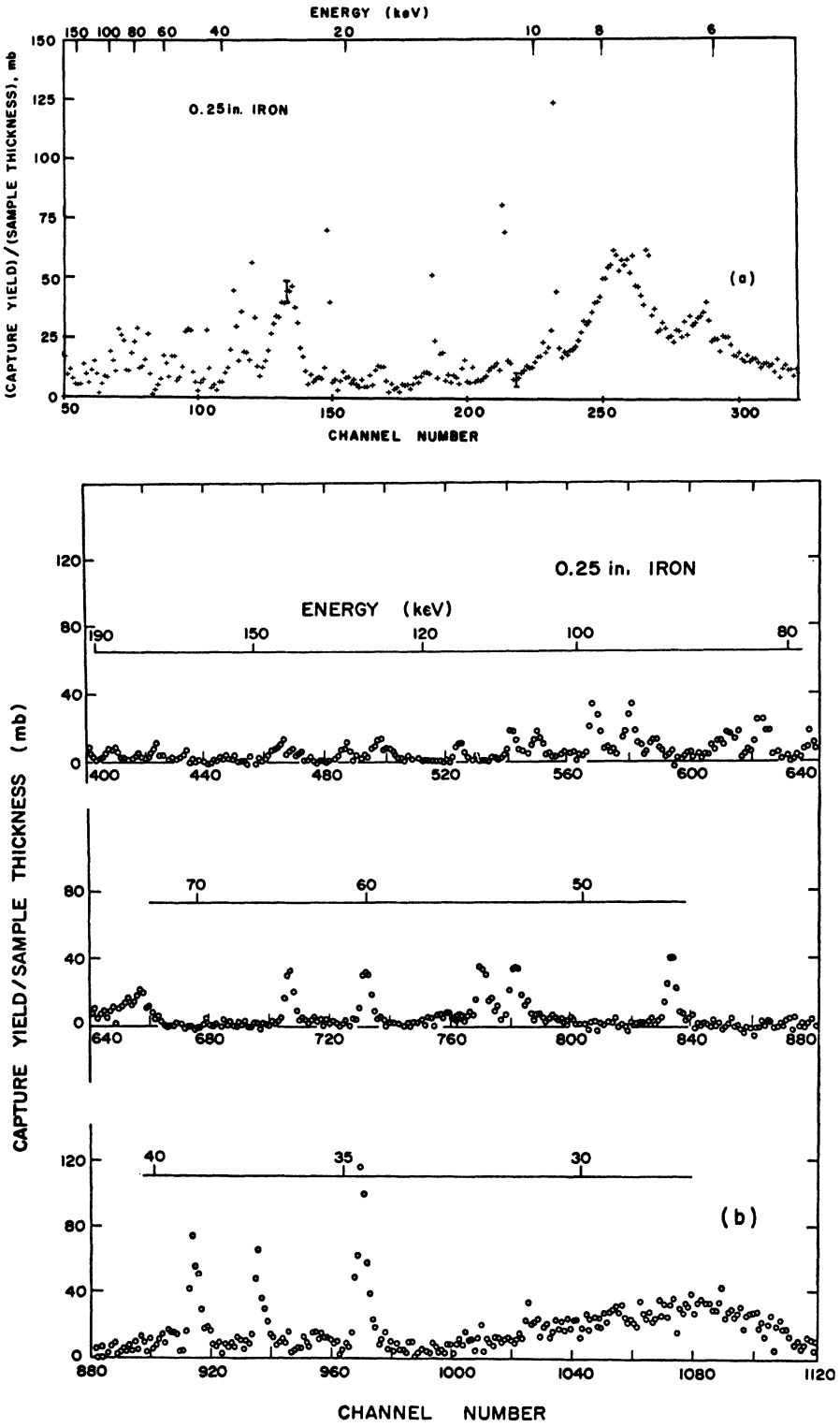

FIG. 7 (a) (Capture yield)/(sample thickness) from 5 to 150 keV for natural Fe for a 0.25-in. sample, 5-nsec/m resolution. (b) (Capture yield)/(sample thickness) from 25 to 200 keV for natural Fe for a 0.25-in. sample, 1.3-nsec/m resolution.

25.44 m. This meant that the neutron flux had to be "compressed" to the 25.44-m path in order that the number of neutrons per time-of-flight channel would correspond to that which would have been measured at this shorter path. An additional correction was made to account for the air path attenuation of neutrons between 25.44 and 28.05 m since this changed by 7.4% for neutron energies between 60 eV and 200 keV.

TABLE IV. Resonance parameters for ^{54}Fe.

E_0 (keV)	N (sample)	A_γ (eV)	$\delta A_\gamma/A_\gamma$ (%)	Multiple captures (%)	Parameters $g(\Gamma_n\Gamma_\gamma/\Gamma)$ (eV)	$\sigma_0\Gamma_\gamma$ (b eV)
7.82						
9.48	1	0.104	±25	<1	0.66	182
	2	0.065	±25	<1	0.38	105
	3	0.71	±10	3	0.52	144
	3	0.71	±10	3	0.53	145
	3	0.64	±10	3	0.48	131
					(0.51±0.05)[a]	(140±14)
					0.6±0.2[b]	
14.4	3	0.53	±25	2	0.60	108
	3	0.42	±25	2	0.47	86
					(0.53±0.14)	(97±25)
52	3	...	...	...	...	...

[a] Because of systematic errors, $[g(\Gamma_n\Gamma_\gamma/\Gamma)]$ is not determined to better than 10%.
[b] Reference 18.

B. Relation of Yield to Resonance Parameters

The yield $Y_{xi}(E)$ was defined by Eq. (1) as the ratio of number of captures to number of incident neutrons.

The primary yield is defined as those capture events which take place at the first collision only. For a unit flux incident on a slab of thickness X, the primary yield between x and $x+dx$ is

$$dY_P(E)=\exp[-\mathfrak{N}x\sigma_{\Delta t}(E)]\mathfrak{N}\sigma_{\Delta\gamma}(E)\,dx, \quad (3)$$

where $\sigma_{\Delta t}(E)$ = Doppler-broadened total cross section, $\sigma_{\Delta\gamma}(E)$ = Doppler-broadened capture cross section, $\mathfrak{N}$ = atoms/cm^3, and E = neutron energy.

The primary yield is obtained by integrating over the sample thickness:

$$Y_P(E)=\int_0^X dY_P(E) \quad (4)$$

$$=[\sigma_{\Delta\gamma}(E)/\sigma_{\Delta t}(E)]\{1-\exp[-\mathfrak{N}X\sigma_{\Delta t}(E)]\}$$

$$=[\sigma_{\Delta\gamma}(E)/\sigma_{\Delta t}(E)]\{1-\exp[-N\sigma_{\Delta t}(E)]\}, \quad (5)$$

where $N=\mathfrak{N}X$.

The capture area under the resonance, A_γ, is obtained by integrating the primary yield[16]:

$$A_\gamma\equiv\int Y_P(E)\,dE$$

$$=\int_{-\infty}^{\infty}\{1-\exp[-N\sigma_{\Delta t}(E)]\}\frac{\sigma_{\Delta\gamma}(E)}{\sigma_{\Delta t}(E)}\,dE. \quad (6)$$

[16] Actually, instrumental resolution should be taken into account. Since only areas A_γ are used in the analysis, the effects of resolution broadening are integrated out and do not affect the interpretation.

For an ideally thin sample (expanding the exponential):

$$A_\gamma=\int_{-\infty}^{\infty}N\sigma_{\Delta\gamma}(E)\,dE. \quad (7)$$

For a thin sample, the area is independent of Doppler broadening, and hence

$$A_\gamma\approx N\int_{-\infty}^{\infty}\sigma_\gamma(E)\,dE=\tfrac{1}{2}\pi N\sigma_0\Gamma_\gamma=2\pi^2\lambda\!\!\!^{-2}Ng\Gamma_n\Gamma_\gamma/\Gamma,$$

where σ_0 is the total cross section at resonance and is equal to $4\pi\lambda\!\!\!^{-2}g\Gamma_n/\Gamma$; $\lambda\!\!\!^{-}$ is the reduced neutron de Broglie wavelength.

C. Multiple Scattering Correction

The primary capture yield in Eq. (5) is the capture yield in the absence of multiple scattering effects. The experimentally observed capture yield will consist of a contribution due to primary neutron captures plus those captures due to multiple interactions of neutrons which have undergone scattering. In the case of the strong 27.7-keV s-wave resonance in ^{56}Fe, the multiple interaction (or multiple scattering) contribution is as large or larger than the primary contribution for a 0.635-cm-thick sample. For such resonances, a Monte Carlo code, written by Sullivan and Warner of the Oak Ridge National Laboratory, was used. With a few minor changes, this code was recompiled for use on the CDC 6600 computer at New York University. Given a set of resonance parameters, this code calculates the primary capture yield, the multiple interaction contribution to the capture yield, and the total capture yield per unit energy bin over a selected energy range. This calculated yield is then compared to the

TABLE V. Resonance parameters for ^{56}Fe.

E_0 (keV)	N (sample)	A_γ (eV)	$\delta A_\gamma/A_\gamma$ (%)	Multiple captures (%)	Parameters $g(\Gamma_n\Gamma_\gamma/\Gamma)$ (eV)	$\sigma_0\Gamma_\gamma$ (b eV)
1.15	1[a]	0.44	±25	2	$g\Gamma_n=0.086$	$+0.021$ -0.014
	2	0.69	±25	2	(Assume $\Gamma_\gamma=0.6$ eV)	
	3	5.54	±8	25	$2g\Gamma_n=0.136\pm0.012$[b]	
					$2g\Gamma_n=0.104=0.010$[c]	
2.35	3	0.033	±25		0.0004	0.43
	3	0.032	±25		0.0004	0.41
					(0.0004)[d]	(0.42)
11.2	1	0.11	±30		0.054	12.6
	2	0.16	±30		0.068	15.9
	3	0.76	±10	5	0.040	9.85
	3	0.74	±10	5	0.041	9.56
	3	0.89	±10	5	0.049	11.5
	4	1.64	±10		0.042	9.81
					(0.043±0.007)	(10.2±1.5)
22.7	1	0.19	±25		0.19	21.4
	2	0.37	±25		0.32	37.7
	3	1.67	±10	½	0.188	21.6
	3	1.75	±10	½	0.197	22.6
	3	1.74	±10	½	0.196	22.5
	4	4.47			0.187	21.4
					(0.191±0.02)	(21.9±2.0)
27.7	1	1.16	±20	20	$\Gamma_\gamma=1.30\pm0.3$	
	2	1.64	±20	20	$\Gamma_\gamma=1.84\pm0.4$	
	3	10.4	±8	50	$\Gamma_\gamma=1.54\pm0.12$	
	3	10.1	±10	50	$\Gamma_\gamma=1.50\pm0.15$	
					($\Gamma_\gamma=1.44\pm0.14$) eV	
					$\Gamma_\gamma=1.5\pm0.3$ eV[e]	
					$\Gamma_\gamma=1.3$ eV[c]	
34.1	3	2.21	±10	4	0.47	35.6
	4	3.89	±10	4	0.71	53.5
					(0.59±0.07)	(44.1±5.0)
36.6	3	1.24	±10	3	0.270	19.2
	4	2.10	±12		0.332	23.7
					(0.301±0.032)	(21.4±2.2)

TABLE V (*Continued*)

E_0 (keV)	N (sample)	A_γ (eV)	$\delta A_\gamma/A_\gamma$ (%)	Multiple captures (%)	Parameters $g(\Gamma_n\Gamma_\gamma/\Gamma)$ (eV)	$\sigma_0\Gamma_\gamma$ (b eV)
38.3	3	1.84	±10	1	0.41	27.8
	4	3.36	±10		0.51	32.4
					(0.46±0.05)	(30.1±3.0)
45.8	3	1.23	±12	1	0.32	18.1
	4	2.61	±10		0.33	19.4
					(0.32±0.04)	(18.7±2.0)
51.9	3	1.73	±10	3	0.51±0.05	25.6±2.6
53.3	3	1.73	±10	3	0.54±0.06	26.4±2.8
55.0	4	0.98	±25		0.14±0.04	6.7±2.0
59.0	3	1.62	±10		0.52	23.3
	4	3.28			0.57	25.1
					(0.54±0.06)	(24.2±2.6)
63.1						
72.6						
74.6						
76.7[f]						
80.4[f]						
82–84 (unresolved)[f]						
90[f]						
92.1[f]						
95.9[f]						
102[f]						
105[f]						
112[f]						
124[f]						
129[f]						

[a] 1 = 6.286×10⁻³ atoms/b
2 = 6.778×10⁻³ atoms/b
3 = 5.370×10⁻³ atoms/b
4 = 0.1610 atoms/b.
[b] Reference 21.
[c] Reference 18.
[d] Mean value.
[e] Reference 23.
[f] Tentatively assigned to ^{56}Fe.

experimental capture yield to obtain the radiation width in the following manner. For the strong scattering resonances, e.g., 27.7 keV in ^{56}Fe and 34.6 keV in ^{27}Al, Γ_n is known from transmission measurements[7] and is also known to be much larger than Γ_γ. Using the known neutron widths, the capture yield is calculated for a range of radiation widths and sample thicknesses. Integrating the calculated capture yield over the resonance, a curve is generated of capture area A_γ versus radiation width. The intercept of the experimental capture yield area on this curve then gives the radiation width. This was done for several sample thicknesses for each resonance and the final value of the radiation width is the weighted mean intercept.

Figure 5 shows an example for the case of the 2.85-keV resonance in Na. The radiation width determined for this resonance is quite insensitive to errors in the neutron width. This may be seen from the limiting case of the thin sample capture area: $A_\gamma \propto \sigma_0\Gamma_\gamma$, which is in turn proportional to $g(\Gamma_n\Gamma_\gamma/\Gamma)$. For these particular levels, since $\Gamma_n \gg \Gamma_\gamma$, $g(\Gamma_n\Gamma_\gamma/\Gamma) \sim g\Gamma_\gamma$, the capture area is directly proportional to the radiation width. This is exactly what is observed in Fig. 5. Several cases were run with the Monte Carlo program to check this, including a variation in neutron width by ±10%.

Since the experimental resolution width was less than the resonance width for some resonances, the shape of the calculated yield could be directly compared with

TABLE VI. Resonance parameters for ^{57}Fe.

E_0 (keV)	N (sample)	A_γ (eV)	$\delta A_\gamma/A_\gamma$ (%)	Multiple captures (%)	Parameters $g(\Gamma_n\Gamma_\gamma/\Gamma)$ (eV)	$\sigma_0\Gamma_\gamma$ (b eV)
1.63	3[a]	0.14	±25	<1	0.046	73.0
	3	0.15	±25	<1	0.051	81.5
	5	0.23	±10	<3	0.053	84.4
					(0.050±0.010)	(79.6±16.0)
3.96	5	0.43	±10	10	$\Gamma_\gamma=1.09\pm0.12$	
	3	0.33	±10	20	$\Gamma_\gamma=1.20\pm0.12$	
					($\Gamma_\gamma=1.14\pm0.06$	Assume $g=\frac{1}{4}$, $\Gamma_n=177$ eV
					$\Gamma_\gamma\leq1.7$[b]	
4.75	5	0.086	±30	<1	0.058	32.0
	3	0.046	±30	<1	0.045	24.8
					(0.051±0.61)	(28±5)
6.21	5	1.00	±10	20	$\Gamma_\gamma=1.32\pm0.12$ -0.14	Assume $g=\frac{3}{4}$, $\Gamma_n=396$ eV
					$\Gamma_\gamma\leq1.7$[b]	
7.22	5	0.36	±30	<1	0.36±0.09	132±33
7.90	5	0.16	±25	<1	0.18±0.05	60±18
12.8	5	0.27	±20	<1	0.50	101.5
	3	0.12	±30	<1	0.33	67.6
					(0.42±0.10)	(84±20)
					1.4±0.4[b]	
					2.0±0.3[c]	
13.9	5	0.40	±20	<1	0.79	148
	3	0.18	±50		0.52	97
					(0.70±0.20)	(122±30)
18.0	3	0.14	±30	<1	0.52±0.16	76.5±25
					2.2±0.6[b]	
					1.5±0.5[c]	
21.3	5	0.36	±25	<1	1.09±0.28	135±32
28.3[d]	5					
29[d]	5	0.76	±20	8	$\Gamma_\gamma=4\pm1$ eV	Assume $g=\frac{3}{4}$, $\Gamma_n=3000$ eV
40	5	...	...		$\Gamma_\gamma=6\pm2$ eV[c]	

[a] 3 = 0.0537 atoms/b, 5 = ^{57}Fe enriched sample, 0.00188 atoms/b.
[b] Reference 18.
[c] Reference 23.
[d] Appears to be p wave superimposed on s-wave resonance.

the experimental results. Good agreement was obtained as is seen for the 27.7-keV ^{56}Fe resonance in Fig. 6.

For the weaker resonances, $\Gamma_n \lesssim \Gamma_\gamma$, and the capture yield was calculated for a range of values of both Γ_n and Γ_γ. These results showed that the multiple scattering correction is small, typically 2–3% or less. This will be discussed in more detail in Sec. IV.

D. Discussion of Errors

The sources of error in this experiment are:

(1) *Capture counting statistics.* The errors quoted in the final results include those contributions due to counting statistics. The magnitude varies with sample thickness. These errors in terms of standard deviations varied from 1 to 30%.

(2) *Efficiency of capture detector.* Since the capture yield is inversely proportional to the efficiency, an error in the efficiency will be reflected in the yield. Any change in the de-excitation scheme from resonance to resonance would have to be quite drastic in order to affect the efficiency determination. The observed capture pulse-height data appear to be quite similar for the various resonances in the same nuclide. The error in the detector efficiency is estimated to be ±5%.

(3) *Sensitivity to scattered neutrons.* For some resonances in the keV region, the neutron widths may be approximately 1000 times larger than the radiation width. Thus, a small scattering sensitivity in the capture detector could cause a scattering background roughly equal to the true capture rate. A separate experiment

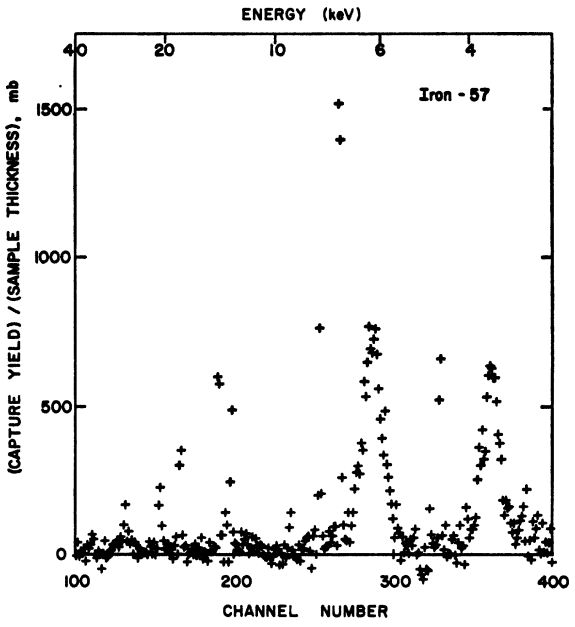

FIG. 8. (Capture yield)/(sample thickness) from 1.5 to 40 keV for ^{57}Fe (0.179 g/cm^2), 5-nsec/m resolution.

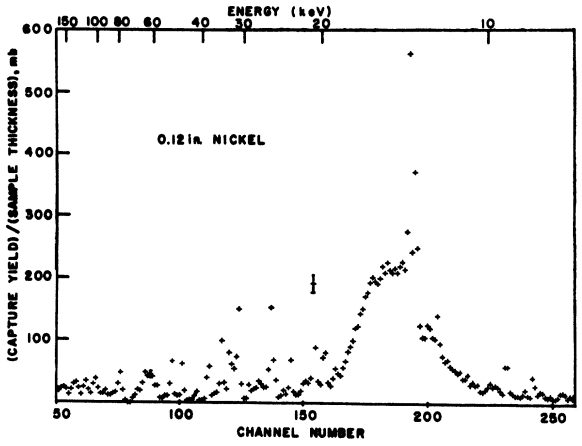

FIG. 9. (Capture yield)/(sample thickness) from 5 to 150 keV for Ni for a 0.12-in. sample, 5-nsec/m resolution.

was performed to measure the neutron scattering sensitivity of the capture detector and is described in Appendix II. The scattering sensitivity was found to be of the order of one part in 100 000.

(4) *Relative neutron flux.* The error in the counting statistics of the data for the relative flux calculation never exceeded ±1½%. The relative efficiency of the $^{10}B_4C$-NaI detector has been discussed. Calculations showed that small differences in the ^{10}B cross section did not make sizable differences in the relative efficiency. (For example, if, at high energy, the ^{10}B absorption cross section is made slightly larger and the ^{10}B scattering cross section is made correspondingly smaller, the two effects tend to cancel each other.) The estimated error for the relative neutron flux is ±2½%.

(5) *Absolute flux normalization.* The absolute flux is determined from the saturated resonance capture in silver near 5.19 eV. Silver was chosen because of its "soft" capture γ spectrum and the predominantly capture resonance at 5.19 eV. Examination of the basic yield equation shows that the capture detector efficiency for Ag and the sample of interest occur as a ratio. Thus, errors in the efficiency calculation tend to cancel out. The counting statistics (typically, 2%) of the 60.2-eV Au resonance were included in the estimates of all the errors. The error in the absolute flux normalization is estimated to be ±4%.

(6) *Monte Carlo calculations.* For those resonances where the radiation width was determined, 1000 neutron histories were run for each set of parameters. Since the code uses the usual weighting procedure in following each neutron history, the "statistics" are considerably better than 3%.

In summary, the contributions of the above sources of error have been included in the quoted errors with some extra allowance made for estimated systematic errors. The error in energy measurements due to timing uncertainties is about 1% at 100 keV and ½% at 1 keV.

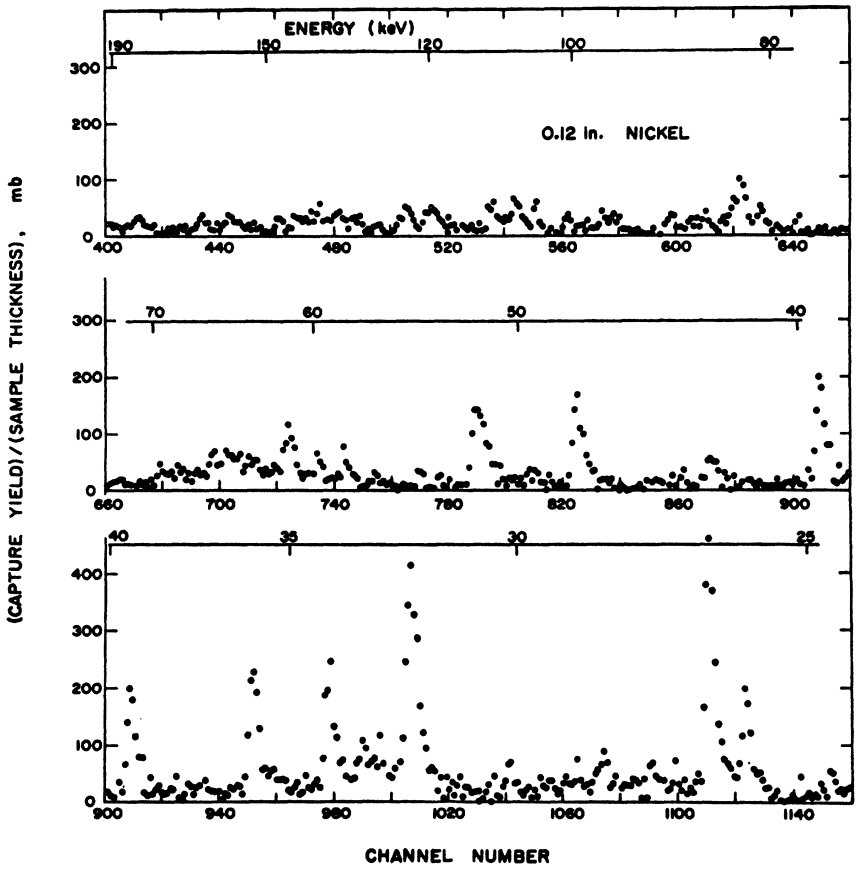

FIG. 10. (Capture yield)/(sample thickness) from 25 to 200 keV for natural Ni for a 0.12-in. sample, 1.3-nsec/m resolution.

IV. RESULTS

A. Iron

Several authors have reported resonances in iron observed in both transmission[17] and capture[18] measurements. The transmission measurements were performed with high resolution from about 5 to 250 keV. The capture measurements covered the energy range from 1 to 50 keV, however, with somewhat poorer resolution. The capture measurements reported here cover the range from about 280 eV to 200 keV, with greater sensitivity for detecting weak resonances than the transmission experiments and better resolution and higher efficiency than the previous capture measurements. Natural iron samples and enriched samples of ^{56}Fe, ^{57}Fe, and ^{58}Fe were used for the isotopic assignment of the resonances observed. Fifty resonances are seen in this capture measurement up to 130 keV compared to about 15 reported from the transmission experiments.[17]

The capture data were reduced to capture yield divided by sample thickness, Y/N, using the method described in Sec. III. Although Y/N has the units of cross section (10^{-24} cm^2), it is very important to note that this quantity is *not* the true capture cross section since the observed capture yield includes the effects of sample self-shielding, multiple scattering, and resolution broadening. *Only in the limiting case of an ideally thin sample and perfect resolution would Y/N be equal to the capture cross section.* Figures 7(a) and 7(b) show the Y/N for a 0.635-cm-thick natural iron sample over the energy ranges from 5 to 150 keV and 24 to 190 keV, respectively. The capture detector efficiency for ^{56}Fe was used for these curves. Time-of-flight channel number is shown on the abscissas with neutron energies noted above. The capture yield shows the well-known broad s-wave levels at 3.9, 6.1, and 28 keV. Most of the remaining resonances are very narrow and hence only the experimental resolution width is observed. Close examination on the high-energy side of some of these resonances reveals a broad "hump" due to neutrons being scattered onto the resonance energy; the peak in this "hump" corresponds to ~90° scattering in the sample. This multiple scattering effect can be removed from the data by a simple shape fit to the resonance in order to extract the resonance capture area. The resonances observed at ~130 and 330 eV

[17] J. B. Garg, J. Rainwater, and W. W. Havens, Jr., Columbia University European and American Nuclear Data Committee Report No. EANDC (US) 54 "L," CR-1860 (unpublished).

[18] M. C. Moxon, in *International Conference on the Study of Nuclear Structure with Neutrons, Antwerp, 1965* (North-Holland Publishing Co., Amsterdam, 1966).

TABLE VII. Resonance parameters for ^{58}Fe.

E_0 (keV)	N (sample)	A_γ (eV)	$\delta A_\gamma/A_\gamma$ (%)	Multiple captures (%)	Parameters $g(\Gamma_n\Gamma_\gamma/\Gamma)$ (eV)	$\sigma_0\Gamma_\gamma$ (b eV)
0.230	3[a]	0.0206	±20	<1	0.0065±0.0014	74.1
0.359	3	0.0343	±15	<1	0.017±0.005	124.
2.82						
4.96						
6.16						
9.29						
10.4						

[a] 3 = 0.0537 atoms/b.

in iron by Mitzel and Plendl[19] are not observed in these data. These resonances were presumably caused by Co and Mn impurities in their iron sample.

The resonances appear to be resolved up to about 70 keV. Above this energy, it becomes difficult to separate levels and match those observed in capture to those seen in transmission measurements. Above 40 keV, these data show a general decreasing trend of Y/N with increasing energy. This trend is in agreement with the slowing-down-time spectrometer results of Isakov *et al.*[20] but is in disagreement with the results of Moxon.[18] These latter results exhibited a slight upward trend to 100 keV. The area of the resonances were determined from the Y/N data with the aid of the IBM 360/50 computer at Rensselaer. Where applicable the values $\sigma_0\Gamma_\gamma$, or $g(\Gamma_n\Gamma_\gamma/\Gamma)$, were obtained from the thin sample approximation (as discussed in Sec. III).

^{54}Fe

Table IV lists the resonance energy, sample thickness, A_γ, per cent error in A_γ, per cent multiple captures, and resonance parameters derived from these data for ^{54}Fe and other author's results. The resonance at 7.82 keV was identified from its presence in the natural iron data and in its absence in the ^{56}Fe, ^{57}Fe, and ^{58}Fe data. However, because of the two ^{57}Fe resonances overlapping the 7.82-keV ^{54}Fe resonance, this resonance was not analyzed for its radiation width. No information on the neutron width is available for the 9.48 and 14.4-keV resonances and thus only $\sigma_0\Gamma_\gamma$ and $g(\Gamma_n\Gamma_\gamma/\Gamma)$ (based on the thin-sample approximation) are presented. However, the $g(\Gamma_n\Gamma_\gamma/\Gamma)$ of the 9.48-keV resonance may be compared to that obtained by Moxon[18] and the agreement is within the statistical errors quoted for both measurements. The ^{54}Fe resonance at 52.1 keV shows up as a broad hump upon which are located two relatively narrow levels in ^{56}Fe.

^{56}Fe

Resonances observed in ^{56}Fe up to 129 keV are listed in Table V. For the 1.15- and 27.7-keV resonances, the Monte Carlo code was used to obtain the resonance parameters, but for the other resonances a combination of analytical and Monte Carlo methods were used.

The radiation width is known[21] to be approximately 0.6 eV for the 1.15-keV resonance. Using this radiation width, $g\Gamma_n$ is determined to be [0.086(+0.021, −0.014) eV], which is in reasonable agreement with previous reported values.[18,22]

The radiation width of the 27.7-keV s-wave resonance was determined using the known neutron width[7] Γ_n = 1670 eV in the Monte Carlo code. This radiation width [1.44±0.14 eV] agrees very well with previously reported values.[18,23] To test the effect of the uncertainty in the neutron widths on the resulting radiation width, the integrated yield A_γ was calculated again with the Monte Carlo code for Γ_n = 1503 and 1837 eV, which are almost equal to the limits of the published experimental error on Γ_n. The radiation width was held constant in both cases. The integrated yield A_γ increased by 2% when the neutron width changed from 1503 to 1837 eV, showing that the results are relatively insensitive to the value of the assumed neutron width. It is interesting to note that the radiation width of this s-wave resonance is about twice as large as that of the 1.15-keV p-wave resonance.

$l \geq 1$ Resonances. If all the resonances in ^{56}Fe are considered to be s wave, over 75% of these resonances have reduced neutron widths less than 1.6% of the average reduced neutron width. A Porter-Thomas[24] distribution for neutron widths predicts fewer than 10% of the levels with widths less than 1.6% of the average. This "excess" of small widths is attributed to

[19] F. Mitzel and H. S. Plendl, Nukleonik **6**, 371 (1964).
[20] A. I. Isakov, Y. P. Popov, and F. L. Shapiro, Zh. Eksperim. i Teor. Fiz. **38**, 989 (1960) [English transl. Soviet Phys.—JETP **11**, 712 (1960)].
[21] R. C. Block, Phys. Rev. Letters **13**, 234 (1964); J. A. Moore, H. Palevsky, and R. E. Chrien, Phys. Rev. **132**, 801 (1963).
[22] R. C. Block, Oak Ridge National Laboratory Report No. ORNL-3778 (unpublished).
[23] R. L. Macklin, P. J. Pasma, and J. H. Gibbons, Phys. Rev. **136**, B695 (1964).
[24] C. E. Porter and R. G. Thomas, Phys. Rev. **104**, 483 (1956).

TABLE VIII. Resonance parameters for ^{58}Ni.

E_0 (keV)	N (sample)	A_γ (eV)	$\delta A_\gamma/A_\gamma$ (%)	Multiple captures (%)	Parameters $g(\Gamma_n\Gamma_\gamma/\Gamma)$ (eV)	$\sigma_0\Gamma_\gamma$ (b eV)
6.89	1[a]	0.18	±11		0.021	7.6
	2	0.31	±8		0.024	9.0
					(0.022±0.002)	(8.3±0.8)
12.6						
13.3	1	1.19	±8		0.34	65.5
	2	1.39	±7		0.31	61.0
					(0.32±0.03)	(63.2±6.0)
13.6	1	1.96	±7		0.55	105
	2	2.36	±6		0.50	97
					(0.52±0.05)	(101±10)
14–16						
16.5						
17.2						
19.0	1	0.21	±36		0.069	9.4
	2	0.22	±12		0.058	7.9
					(0.063±0.010)	(8.7±1.3)
20.0	1	0.61	±11		0.026	26.9
	2	0.79	±8		0.194	25.2
					(0.20±0.02)	(26.0±2.7)
21.1	1	1.68	±9		0.59	72.4
	2	2.17	±7		0.54	67.0
					(0.56±0.06)	(70±7)
26.6	1	1.93	±9	1	0.75	74.0
	2	2.4	±7	7–8	0.64	63
					(0.70±0.07)	(68±7)
32.4	1	2.98	±9	1½	1.49	120
	2	3.97	±7		1.34	108
					(1.44±0.15)	(114±12)
34.2	1	1.48	±10	1	0.70	53.5
	2	1.82	±8	5–9	0.60	45.5
					(0.65±0.08)	(49.5±5.0)
36.1	1	1.92	±7	1–1½	0.95	68.5
	2	2.47	±8	7–12	0.78	57.0
					(0.86±0.10)	(62±7)
39.5						
47.9	1	2.00	±10	1½	1.61	87.6
	2	2.67	±8	4	1.55	87.4
					(1.58±0.18)	(87.5±11.0)

TABLE VIII (*Continued*)

E_0 (keV)	N (sample)	A_γ (eV)	$\delta A_\gamma/A_\gamma$ (%)	Multiple captures (%)	Parameters $g(\Gamma_n\Gamma_\gamma/\Gamma)$ (eV)	$\sigma_0\Gamma_\gamma$ (b eV)
52.1	1[a]					
	2					
54.8	1	0.26	±27		0.25	11.8
	2	0.60	±26		0.44	20.6
					(0.32±0.10)	(16.2±5.0)
60.1[b]						
61.8						
66.4						
78.2[b]						
81.3[b]						
83.0						
95.9						
101[b]						
105[b]						
107[b]						
110						
120[b]						
124[b]						

[a] 1 = 0.028898 atoms/b, 2 = 0.04811 atoms/b. [b] Observed in natural Ni sample.

p-wave levels, and these small levels have accordingly been treated as p wave. Since these resonances in ^{56}Fe have small neutron widths, it becomes difficult to make comparisons with other investigators since they usually lacked adequate resolution or sensitivity to separate the resonances.

The multiple scattering effects were calculated with the Monte Carlo code for several of the weaker resonances and it was found that this effect was generally less than 5%. (For this purpose, the code had to be changed to represent p-wave resonances.) Since the multiple scattering was so small, it was possible by using the computed results from selected resonances to analytically correct the remaining resonance for multiple scattering and sample thickness effects to obtain a value of $g(\Gamma_n\Gamma_\gamma/\Gamma)$. The total correction varied between 2 and 7%. If one assumes that the radiation width is constant and equal to 0.6 eV for these p-wave resonances, the largest possible value of $g(\Gamma_n\Gamma_\gamma/\Gamma)$ is equal to $0.6g$. This is readily seen by noting that if $\Gamma_n \gg \Gamma_\gamma$, then $g(\Gamma_n\Gamma_\gamma/\Gamma)$ reduces to $g\Gamma_\gamma$, but if $\Gamma_n \ll \Gamma_\gamma$, then $g(\Gamma_n\Gamma_\gamma/\Gamma)$ reduces to $g\Gamma_n$, which is less than $g\Gamma_\gamma$. For a p-wave resonance in ^{56}Fe, the spin factor g can be 1 or 2. With this information, one can say that for the 2.35-, 11.2-, and 22.8-keV resonances, $g(\Gamma_n\Gamma_\gamma/\Gamma) \approx g\Gamma_n \approx \Gamma_n$ or $2\Gamma_n$. For the other ^{56}Fe resonances, the value of $g(\Gamma_n\Gamma_\gamma/\Gamma)$ only shows that $\Gamma_n \gtrsim \Gamma_\gamma$.

Furthermore, with the assumptions that $\Gamma_\gamma = 0.6$ eV and $l=1$ for these resonances, one can calculate the reduced neutron width and level spacing for these resonances. From this, one can then obtain the p-wave strength function. The broad resonances observed in ^{56}Fe in transmission below 70 keV are known to be s wave by the characteristic resonance-potential scattering interference and can be excluded from this calculation. For the remaining levels, defining the reduced neutron width as $\Gamma_n^1 = \Gamma_n/(E_0)^{1/2}v_1$ for p-wave resonances, where E_0 is the resonance energy and v_1 is the penetrability factor for $l=1$, the p-wave strength function is calculated from the relation[25]

$$S^1 = [1/3(E_2 - E_1)] \sum_i [(g\Gamma_n)_i/(E_{0i})^{1/2}v_1], \quad (9)$$

where the sum includes all the p-wave resonances.

The p-wave strength function is found to be $(0.10 \pm 0.04) \times 10^{-4}$ for ^{56}Fe, which is considerably lower than the optical-model value[5] of about 1.4×10^{-4}. In fact, since it is quite possible that one or more of the weak resonances might be due to s-wave neutrons, this value of the p-wave strength function is if anything too large. It is of course possible (in fact probable) that some of the p-wave resonances are not detected, but these represent the weaker resonances which do not contribute

[25] A. Saplakoglu, L. M. Bollinger, and R. E. Cote, Phys. Rev. **109**, 1258 (1958); C. Lubitz and T. Reynolds (private communication).

TABLE IX. Resonance parameters for ^{60}Ni.

E_0 (keV)	N (samples)	A_γ (eV)	$\delta A_\gamma/A_\gamma$ (%)	Multiple captures (%)	Parameters $g(\Gamma_n\Gamma_\gamma/\Gamma)$ (eV)	$\sigma_0\Gamma_\gamma$ (b eV)
1.294	1[a]					
2.26	1	0.68	±7		0.063	73.2
	2	1.11	±8		0.068	78.2
					(0.065±0.007)	(75.7±8.0)
5.52	1	0.23	±10		0.059	27.9
	1	0.20	±12		0.051	23.9
					(0.055±0.006)	(25.9±3.0)
12.2	1	0.22	±12		0.16	34
	2	0.29	±8		0.19	40
					(0.17±0.02)	(37±4)
13.8						
12–14	(Not resolved)					
23.8	1	0.88	±12		0.84	92.0
	2	1.11	±10		0.725	79.4
					(0.78±0.10)	(85.7±12.2)
28.5	1	0.22	±18		0.27	24.9
	2	0.26	±21		0.25	22.6
					(0.26±0.05)	(23.2±5.0)
30.2	1	0.16	±22		0.200	17
	2	0.55	±13		0.48	41
					(0.39±0.06)	(33±5)
33.4						
39.5						
42.9	1	0.43	±16		0.70	43
	2	0.85	±14		0.84	51
					(0.77±0.12)	(47±6)
51.9						
57.0						
65.2						
72.8						
87.0						
97.2						

[a] 1 = 0.028898 atoms/b, 2 = 0.04811 atoms/b.

significantly to the p-wave strength function. It is interesting to note that near the iron mass region, $A\approx50$, the p-wave strength function is at a minimum. In the mass region near $A\approx160$, the p-wave strength function is also near a minimum, and the experimental values[26] of the $A\approx160$ strength function also lie well below those predicted by theory. The theoretical and experimental values tend to agree at the peak of the p-wave strength function at $A\approx90$.

Macklin *et al.*[23] has suggested that these resonances are d wave in character, since $A\approx50$ is near the maximum in the d-wave strength function. However, computing the d-wave strength function for these resonances in a similar manner yields a value one order of magni-

[26] B. Buck and F. Perey, Phys. Rev. Letters **8**, 444 (1962).

TABLE X. Resonance parameters for ^{61}Ni.

E_0 (keV)	N (sample)	A_γ (eV)	$\delta A_\gamma/A_\gamma$ (%)	Multiple captures (%)	Parameters $g(\Gamma_n\Gamma_\gamma/\Gamma)$ (eV)	$\sigma_0\Gamma_\gamma$ (b eV)
1.354	1[a]	0.20	±8		0.24±0.03	478±60
2.35						
3.14	1	0.027	±33		0.081	68
	2	0.041	±17		0.088	73.0
					(0.084±0.018)	(71±14)
3.30	1	0.19	±8		0.56	445.
	1	0.11	±14		0.34	275
	2	0.17	±10		0.53	302
					(0.48±0.06)	(341±44)
6.47	1	0.45	±80		0.15	61
	2	0.07	±25		0.32	128
		0.09	±23		0.40	163
					(0.35±0.10)	(145±43)
7.12	2	0.17	±15		0.78±0.12	285±42
7.53						
8.71	1	0.11	±15		0.76	229
	2	0.11	±16		0.54	162
					(0.65±0.13)	(196±38)
9.90						
10.2						
12.6						
14.0						
14.3						
15.3						
16.7						
17.8						
19.0						
20.4						
24.8	1	0.24	±19		5.14	552
	2	0.19	±28		2.83	297
					(3.98±1.3)	(425±120)
27.6	1	0.055	±40		1.25	118
	2	0.15	±40		2.23	211
					(1.74±0.85)	(164±80)
29.0						
30.8						
31.7						
33.8						
37.3						
41.3						
46.1						
50.7						
58.7						
70.8						
89.6						

[a] 1 = 0.028898 atoms/b, 2 = 0.04811 atoms/b.

TABLE XI. Resonance parameters for ^{62}Ni.

E_0 (keV)	N (sample)	A_γ (eV)	$\delta A_\gamma/A_\gamma$ (%)	Multiple captures (%)	Parameters
2.34					
4.6	1[a]	0.399	±10	37	$\Gamma_\gamma=0.76\pm0.12$ eV
					Assume: $\Gamma_n=1300$ eV[b]
					$g=1$

[a] 0.028898 atoms/b. [b] Reference 7.

tude larger than that expected from theory. In fact, the "strength" of the single smallest observed resonance is adequate to account for the entire calculated d-wave strength function and it is concluded that these resonances are due to p-wave neutrons.

^{57}Fe

The resonances observed in ^{57}Fe are listed in Table VI. Resonance parameters are listed where the neutron widths were known. The values of $\sigma_0\Gamma_\gamma$ and $g(\Gamma_n\Gamma_\gamma/\Gamma)$ are in good agreement where it is possible to make a comparison with other resolved data. For the resonances above 8 keV, the differences between these results and those of Moxon[18] and Macklin *et al.*[23] are attributed to the better resolution of the present data. A new resonance was observed at 7.9 keV in this experiment. The resonance at 7.22 keV has been assigned to ^{57}Fe, in disagreement with Moxon's[18] assignment to ^{54}Fe. The ^{57}Fe data at 28 keV show a narrow resonance superimposed on a wide resonance which is probably the 3-keV-wide resonance reported by Macklin *et al.*[23] (See Fig. 8.) The counting statistics are not adequate to separate what appears to be a narrow resonance at this energy but this narrow resonance is at least an order of magnitude smaller than the 3-keV-wide resonance.

^{58}Fe

The quantities $\sigma_0\Gamma_\gamma$ and $g(\Gamma_n\Gamma_\gamma/\Gamma)$ are listed for two resonances in Table VII along with the energies of other resonances observed in ^{58}Fe. No other information could be obtained from the natural samples for these resonances. Assuming that the radiation width of the 230- and 359-eV resonances is of the order of 1 eV, then $g(\Gamma_n\Gamma_\gamma/\Gamma)\approx g\Gamma_n$ for these levels.

B. Nickel

The capture yield divided by sample thickness of nickel (Figs. 9 and 10) shows a similar level structure to that of iron. The detector efficiency for ^{60}Ni was used in these calculations. Large s-wave resonances are observed along with many narrow resonances which are assigned to p-wave neutrons. The analysis of nickel is complicated by a closer level spacing than iron. In addition, comparison of the present data to other data is made even more difficult by the errors in energy measurements which may be present. Another complication arises due to cobalt which is often present as an impurity and may contribute some structure at low energies, as seen in the peak at ~130 eV in the capture data of Kapchigashev and Popov.[27]

The Ni resonances have been analyzed in the same manner as iron (see previous section). Both Monte Carlo and semianalytical Monte Carlo methods were applied to extract the resonance parameters. These parameters are listed in Tables VIII through XII. A radiation width of 0.76 eV was obtained for the 4.6-keV resonance in ^{62}Ni. Unfortunately, there are no other reported radiation widths or capture areas that can be compared with the results of this experiment. In addition, the region from 12 to 15 keV cannot be resolved owing to the overlapping broad resonances. Enriched samples will be needed for accurate capture measurements in this energy region.

As in iron, there is an excess of small resonances and these are assigned to p-wave neutrons. The p-wave strength function for ^{58}Ni is computed to be $(0.04\pm0.03)\times10^{-4}$. This result agrees with that for ^{56}Fe in that the experimentally determined p-wave strength function is lower than that predicted by theory for $A\approx50$.

C. Sodium

2.85-keV Resonance

Four samples, 2.031×10^{-3}, 2.855×10^{-3}, 6.432×10^{-3}, and 11.165×10^{-3} atoms/b thick, respectively, were used in the capture measurements of this resonance. The capture yield was calculated using the Monte Carlo code for each sample, using the published values of the resonance parameters: $E_0=2850$ eV, $g=\frac{3}{8}$, $\Gamma_n=410$ eV.[28] The radiation width was varied in steps from 0.1 to 6.4 eV for each calculation. The calculated yield and experimental yield are shown in Fig. 11 for the 6.432×10^{-3} atom/b sample. The shape of the calculated yield is in satisfactory agreement with the experimental yield data. Preliminary results seemed to show that the

[27] S. V. Kapchigashev and Yu. P. Popov, At. Ener. **15**, 120 (1963).

[28] M. C. Moxon and N. J. Pattenden, *Nuclear Data For Reactors* (International Atomic Energy Agency, Vienna, 1967), Vol. I, p. 129.

TABLE XII. Resonance parameters for ^{64}Ni.

E_0 (keV)	N (sample)	A_γ (eV)	$\delta A_\gamma/A_\gamma$ (%)	Multiple captures (%)	Parameters $g(\Gamma_n\Gamma_\gamma/\Gamma)$ (eV)	$\sigma_0\Gamma_\gamma$ (b eV)
9.52	1[a]	0.182	±15		1.56	427
	2[b]	0.338	±10		1.90	519
					(1.73±0.20)	(473±70)
26.0						
39.2						
46.1						
53.9						
64.0						
83.4						

[a] 0.028898 atoms/b. [b] 0.04811 atoms/b.

low-energy side of this resonance was higher than the calculated values; however, a review of the background, statistics, and resolution indicate that the calculated and experimental values do agree to within counting statistics. The experimental resolution is slightly larger that the energy bins of the Monte Carlo results, thus causing the experimental values to be higher on both sides of the resonance. This resonance is exceptional in that its neutron width is large in relation to its resonance energy. This means, since $\Gamma_n \propto (E)^{1/2}$, that Γ_n will vary appreciably over the resonance and this must be included in the calculations.

In order to test the effect of the uncertainty in Γ_n upon the final value of the radiation width, two cases were run in the Monte Carlo code in which $\Gamma_\gamma=0.6$ eV and $\Gamma_n=360$ and 450 eV, respectively, the limits of experimental uncertainty. The computed capture area changed by $(1.3\pm1.5)\%$, where the accuracy is determined by the Monte Carlo technique, thus showing that the radiation width obtained is quite insensitive to the value of the neutron width.

The experimental capture yield was calculated for several samples, using limiting values of the background. This procedure gave upper and lower limits on the capture area, and thus the radiation width, and it also gives one a better estimate of the accuracy of the final result. The value of the radiation width of the 2.85-keV resonance is 0.61 ± 0.06 eV, where the error includes contributions from the capture detector efficiency, capture background, capture counting statistics, and the neutron flux. This radiation width is in excellent agreement with that obtained by Moxon[28] ($\Gamma_\gamma=0.6$ eV). However, it should be noted that the thermal absorption cross section calculated from this radiation width is larger than the measured value.

Resonances above 2.85 keV

The results are listed in Table XIII for the sodium resonances observed in this experiment. The 7.53-keV level was first observed in this capture measurement. Assuming a radiation width equal to or greater than 0.6 eV, then $g(\Gamma_n\Gamma_\gamma/\Gamma)\approx g\Gamma_n$ which is equal to 0.0049 eV. For a p-wave resonance in Na, the spin factor g can be $\frac{3}{8}$, $\frac{5}{8}$, or $\frac{7}{8}$. The resulting values of Γ_n are 0.0131, 0.0078, or 0.0056 eV, respectively. A similar argument against d-wave assignment can be applied to this resonance as has been applied to the narrow resonances observed in iron. If this 7.53-keV resonance were a d-wave resonance, it would lead to a d-wave strength function about an order of magnitude larger than is expected.

The 35.0-keV resonance has only recently been observed in thick sample (17.5 gm/cm^2) transmission measurements[29] while the 52.2-keV resonance is more easily observed owing to its large neutron width. However, the resonance capture areas of these two resonances are comparable, showing that resonances

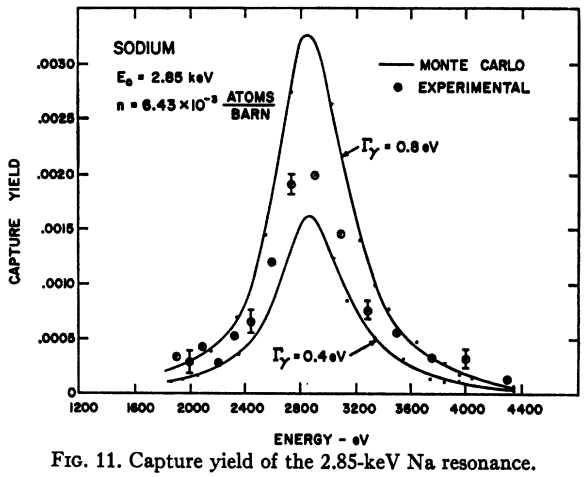

FIG. 11. Capture yield of the 2.85-keV Na resonance.

[29] C. LeRigoleur, J. C. Bluet, and J. L. Leroy, in *International Conference on the Study of Nuclear Structure With Neutrons, Antwerp, 1965* (North-Holland Publishing Co., Amsterdam, 1966).

TABLE XIII. Resonance parameters for sodium.

E_0 (keV)	N (sample)	A_γ (eV)	$\delta A_\gamma/A_\gamma$ (%)	Multiple captures (%)	Parameters $g(\Gamma_n\Gamma_\gamma/\Gamma)$ (eV)	$\sigma_0\Gamma_\gamma$ (b eV)
2.85	1[a]	0.669	±15	20	$\Gamma_\gamma=0.66\pm0.010$	Assume: $g=\frac{3}{8}$ $\Gamma_n=410$ eV
	2	0.914	±15	25	$\Gamma_\gamma=0.66\pm0.010$	
	3	1.864	±15	40	$\Gamma_\gamma=0.61\pm0.009$	
	4	2.673	±15	50	$\Gamma_\gamma=0.52\pm0.008$	
					$\Gamma_\gamma=(0.61\pm0.06)$ eV	
					$\Gamma_\gamma=0.6$ eV[b]	
7.53	6	0.077	±23		0.0040	1.36
	7	0.163	±21		0.0058	2.00
					(0.0049±0.0011)	(1.68±0.35)
35.0	5	0.68	±15		0.283	21.0
	6	2.01	±12		0.461	34.4
	7	2.70	±12		0.438	32.4
					(0.394±0.048)	(29.3±3.5)
						Assume: $\Gamma_n=700$ eV
52.2	5	1.59	±15	±15	$\Gamma_\gamma=1.12$	$g=7/8$
	6	2.42	±16		$\Gamma_\gamma=1.58$	$g=5/8$
	7	2.12	±15		$\Gamma_\gamma=2.60$	$g=3/8$
114.7	6	2.02	±30		1.48	33.5
	7	2.99	±25		1.51	33.8
					(1.50±0.37)	(33.7±8.4)
129.5	6	0.45	±30		0.37	7.40
	7	0.36	±25		0.21	4.07
					(0.29±0.07)	(5.74±1.44)
139.1	6	0.83	±30		0.73	13.8
	7	1.12	±25		0.70	12.7
					(0.71±0.18)	(13.2±3.3)

[a] 1 = 0.00203 atom/b
2 = 0.00285 atom/b
3 = 0.00643 atom/b
4 = 0.01116 atom/b
5 = 0.02197 atom/b
6 = 0.04179 atom/b
7 = 0.06377 atom/b.

[b] Reference 28.

which may be missed in transmission measurements can make significant contributions to capture.

The 52.2-keV resonance is known to be a p-wave resonance with $g\Gamma_n$ equal to about 700 eV.[28,30] The radiation width obtained for this resonance is listed in Table XIII for the three possible spin values. The parameters for the remaining resonances indicate that $\Gamma_n\sim\Gamma_\gamma$.

[30] J. B. Garg, J. Rainwater, S. Winchank, and W. W. Havens, Jr., in *International Conference on the Study of Nuclear Structure With Neutrons, Antwerp, 1965* (North-Holland Publishing Co., Amsterdam, 1966).

D. Aluminum

The Y/N data for aluminum are shown in Fig. 12. Two sample thicknesses were used to determine the radiation widths for the 5.88- and 35.0-keV aluminum resonances. The neutron width is known for the 5.88-keV p-wave resonance[31]; using the values $\Gamma_n=20$ eV and $E_0=5880$ eV, the Monte Carlo code was used to obtain the radiation width from the capture area. Since g, for Al, can be equal to $\frac{3}{12}$, $\frac{5}{12}$, $\frac{7}{12}$, or $\frac{9}{12}$ for a

[31] W. M. Good, J. H. Neiler, and J. H. Gibbons, Phys. Rev. 109, 926 (1958).

TABLE XIV. Resonance parameters of aluminum.

E_0 (keV)	N (sample)	A_γ (eV)	$\delta A_\gamma/A_\gamma$ (%)	Multiple captures (%)	Parameters	
					Assume $\Gamma_n=20$ eV[b]	
5.88	1	1.99	±10	10	$\Gamma_\gamma=0.95$	$g=3/12$
	2	5.64	±10	15	$\Gamma_\gamma=0.57$	$g=5/12$
					$\Gamma_\gamma=0.41$	$g=7/12$
					$\Gamma_\gamma=0.32$	$g=9/12$
35.0	1	5.66	±10	25	Assume $\Gamma_n=1700$ eV[b], $g=7/12$	
	2	17.70	±10	45	$\Gamma_\gamma=(2.8\pm0.3)$ eV	

[a] 1 = 0.03722 atoms/b
2 = 0.11773 atoms/b.

[b] Brookhaven National Laboratory Report No. BNL 325, 2nd ed., Suppl. 2, Vol. I (unpublished).

p-wave resonance, the radiation width corresponding to each possible value is listed in Table XIV.

Similarly, for the 35-keV s-wave resonance, Γ_n was taken to be[32] 1700 eV and $g=\frac{7}{12}$, resulting in a radiation width of $\Gamma_\gamma=2.8\pm0.3$ eV. It is interesting to note that the radiation widths are different by at least a factor of 2 for these two aluminum resonances. Since the 5.88-keV resonance is a p-wave resonance, while the 35-keV level is s wave, these results lead to a conclusion that the radiation width in aluminum is different for an s- and p-wave resonance.

V. CONCLUSIONS

The present experiment has detected considerably more resonance structure in iron and nickel than previously observed. Where comparisons of radiation widths and/or capture areas can be made, the agreement between the present results and other workers is generally satisfactory.[33] The data obtained for iron and aluminum seem to show a difference between s- and p-wave radiation widths. Combining the present capture data and preliminary self-indication data[34] has shown that the 36.6- and 45.8-keV ^{56}Fe resonances may have radiation widths even smaller than the 1.15-keV p-wave[35] resonance.

Generally, for heavier nuclei, the level density is such that there are many ways for an excited nucleus to decay. For this reason one expects the total radiation width to be fairly constant from resonance to resonance. (Julien[36] reports exceptions to this in mercury). However, for lighter nuclei, since there are fewer states available, and hence large fluctuations, the total radiation width may be expected to differ from one resonance to another. Radiation widths may also differ for s- and p-wave resonances since there is a change in parity which may affect the relative number of $E1$ and $M1$ transitions.

The p-wave neutron strength functions obtained for ^{56}Fe and ^{58}Ni are consistent with the trend towards a minimum in this mass region. A value of $[0.3(+0.18, -0.14)]\times10^{-4}$ has recently been obtained for the p-wave strength function[37] for natural Cu, confirming this low trend. {*Note added in proof.* It has been brought to the attention of the authors that low values of

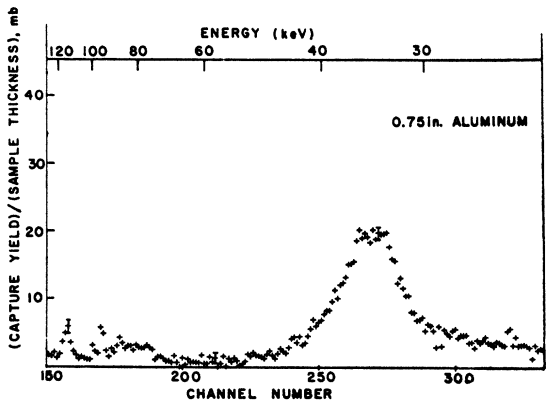

FIG. 12. (Capture yield)/(sample thickness) for Al from 20 to 120 keV for a 0.75-in. sample, 2.5-nsec/m resolution.

[32] C. T. Hibdon, Phys. Rev. **114**, 179 (1959).

[33] A value of $\Gamma_\gamma=0.34$ eV has recently been obtained for the 2.85-keV Na resonance by S. J. Friesenhahn, W. M. Lopez, F. H. Frohner, A. D. Carlson, and D. G. Costello, in *Neutron Cross Sections and Technology, Washington, 1968* (U.S. Government Printing Office, Washington, D.C., 1968), NBS Special Publication 299, Vol. I, p. 533.

[34] J. R. Tatarczuk, R. C. Block, R. W. Hockenbury, and W. R. Moyer, Bull. Am. Phys. Soc. **12**, 512 (1967).

[35] The p-wave nature of this resonance was recently confirmed by A. Asami, M. E. Moxon, and W. E. Stein at the Harwell Laboratory (private communication) and J. Julien at the Saclay Laboratory (private communication); and R. E. Chrien, O. A. Wasson, and D. I. Garber, Bull. Am. Phys. Soc. **13**, 720 (1968).

[36] J. Julien, Ref. 18, p. 156.

[37] H. Weigmann, J. Winter and H. Schmid, in *Neutron Cross Sections and Technology, Washington, 1968* (U.S. Government Printing Office, Washington, D.C., 1968), NBS Special Publication 299, Vol. I, p. 533.

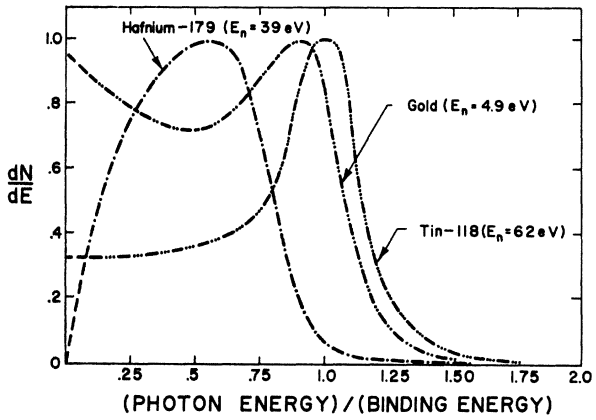

FIG. 13. Capture-γ pulse-height spectra of Au, ^{118}Sn, and ^{179}Hf.

the p-wave strength function are predicted by P. A. Moldauer [Nucl. Phys. **47**, 65 (1963)] and A. P. Jain [Nucl. Phys. **50**, 157 (1964)] in the mass region near atomic weight 50. The low results of this experiment are in general agreement with their predictions.}

ACKNOWLEDGMENTS

We wish to acknowledge the assistance of the Oak Ridge National Laboratory in providing the samples and the capture detector. Discussions with Dr. J. G. Sullivan concerning the Monte Carlo Code were very helpful. One of the authors, R. C. Block, wishes to thank the Oak Ridge National Laboratory for the opportunity of being a member of the laboratory during the initial phases of this research, and to personally thank Dr. J. L. Fowler and Dr. J. A. Harvey of the Oak Ridge National Laboratory (ORNL) Physics Division for their encouragement and support.

The active cooperation, encouragement, and advice of the late Dr. J. E. Russell during the early stages of this work are gratefully acknowledged. The help of all the members of the Nuclear Structure group, the Linac Operating Staff and the machine shop staff are also appreciated.

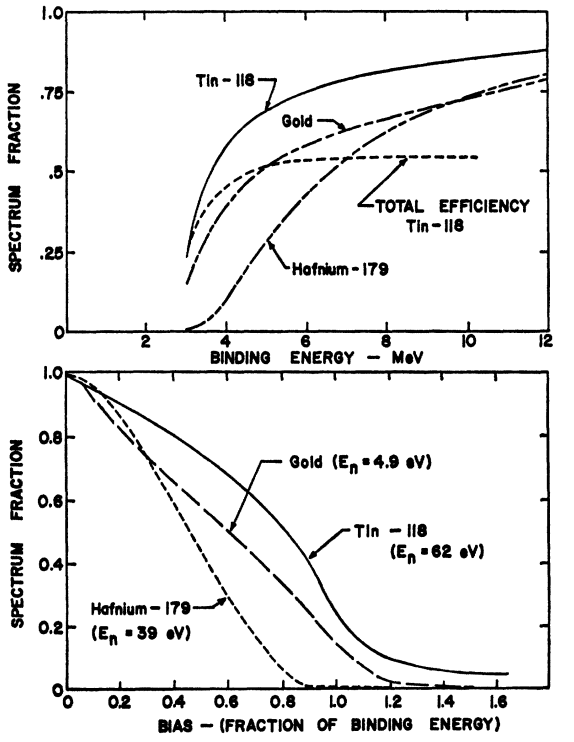

FIG. 14. Spectrum fraction of Au, ^{118}Sn, and ^{179}Hf.

APPENDIX I: CAPTURE-DETECTOR EFFICIENCY

Typical capture-γ pulse-height spectra may be divided into three classes:

(1) Hard—Most of the transitions go directly to or near the ground state. For example: capture in ^{56}Fe resonances, the 62-eV resonance in ^{118}Sn.

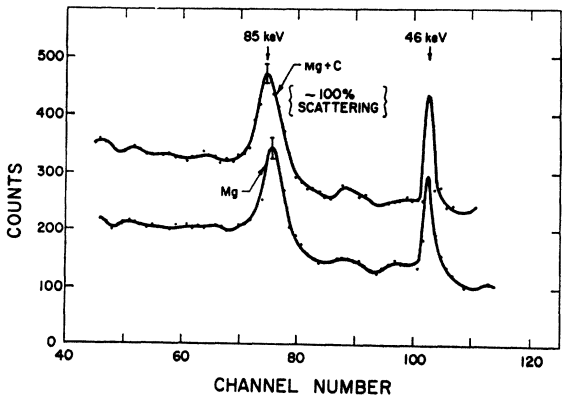

FIG. 15. Neutron capture in Mg with and without carbon-scattering sample.

(2) Soft—Several ($\gtrsim$3) photons are emitted, on the average, after each capture. The average energy per photon is only a small fraction of the binding energy. For example: capture in ^{179}Hf resonances.

(3) Mixture of (1) and (2)—The cascade scheme is a combination of high-energy transitions and high-multiplicity low-energy transitions. For example: capture in Au resonances.

Figure 13 shows the pulse-height spectra of resonance capture in Au, ^{179}Hf, and ^{118}Sn, normalized in terms of γ-ray energy divided by binding energy. Figure 14 shows the spectrum fraction as a function of bias for the three types of spectra in the 1.25-m capture detector. The bias is also expressed in bias energy divided by binding energy for convenience. For a 3-MeV bias, the spectrum fraction versus binding energy is plotted in Fig. 14. Also shown in Fig. 14 is the total efficiency for the hardest observed capture spectrum, capture in the 62-eV resonance of ^{118}Sn. It is interesting to note that the total efficiency remains constant with increasing

binding energy for hard spectra. This occurs because (1) the spectrum fraction increases with increasing binding energy and (2) for hard spectra the intrinsic efficiency (i.e., "stopping power" of the detector) decreases as the binding energy increases. This was confirmed by the experimental results as shown in the spectrum fraction of Fe and Ni in Table III.

The other interesting feature of these results is that, knowing the binding energy and the type of capture pulse-height spectra, one can obtain a fairly accurate spectrum fraction without actually measuring the spectra. Limits can be placed on the efficiency using Fig. 14 since the three classes of spectra represent most cases observed in practice.

APPENDIX II: NEUTRON SENSITIVITY OF THE CAPTURE DETECTOR

In the keV-energy region, some resonances have neutron widths of the order of several keV while the radiation widths are not expected to exceed a few eV. Thus in a typical resonance, the neutron scattering at resonance may be several thousands (or tens of thousands) times stronger than capture, so that any small scattering sensitivity in the large detector could produce a scattering background comparable to the capture signal. In order to establish an upper limit to the scattering sensitivity, the following experiment was performed. It was noted in the measurement of capture in a $\frac{1}{4}$-in.-thick Mg sample that a strong resonance was observed at 85 keV, due to capture in a resonance in ^{24}Mg and a resonance in ^{25}Mg. Since both of these nuclei have a resonance near this energy and each resonance has a neutron width $\approx$8000 times the radiation width, this doublet is ideally suited as a probe for measuring scattering sensitivity. In the lower curve of Fig. 15 are plotted the capture counts per channel versus time-of-flight channel number for capture in the Mg sample. At the wings of the resonance the Mg is scattering only $\approx$15% of the beam into the large scintillator, but at resonance practically 100% of the beam is scattered into the scintillator. If a pure (i.e., no capture) scattering sample is placed behind the Mg sample inside the detector, then the amount of scattering in the wings of the Mg resonance can be increased, but the amount of scattering at resonance is already 100% and cannot increase. This experiment was performed by placing a 4-in.-thick pure carbon scatterer about 3 in. behind the Mg; with this geometry practically 100% of the beam is scattered into the scintillator at all neutron energies. Thus, for example, if the resonance structure observed in the lower curve of Fig. 15 were due to prompt scattering only, then the addition of the carbon would essentially raise the counts in the wings only and the resonance structure would completely disappear. The data are plotted in Fig. 15, and it is noted that the resonance structure does not at all disappear. The addition of the carbon scattering raises the whole curve, but this is due to neutrons which were scattered into the detector from earlier time of flight and are not correlated with prompt scattering. The two resonance areas are the same to within an accuracy of 8%, so therefore the scattering sensitivity of the detector to prompt-scattered neutrons is $\approx 0.08 \times 1/8000 \approx 1/100\,000$.